Distinct kinetic and mechanical properties govern ALCAM-mediated interactions as shown by single-molecule force spectroscopy

Joost te Riet[1,2], Aukje W. Zimmerman[1], Alessandra Cambi[1], Ben Joosten[1], Sylvia Speller[2], Ruurd Torensma[1], Frank N. van Leeuwen[1], Carl G. Figdor[1,*] and Frank de Lange[1,3,‡]

[1]Department of Tumour Immunology (278), Nijmegen Centre for Molecular Life Sciences (NCMLS), Radboud University Nijmegen Medical Centre, PO Box 9101, 6500HB Nijmegen, The Netherlands
[2]Department of Scanning Probe Microscopy, Institute for Molecules and Materials (IMM), Radboud University Nijmegen, PO Box 9010, 6500GL Nijmegen, The Netherlands
[3]Department of Cell Biology (283), Nijmegen Centre for Molecular Life Sciences (NCMLS), Radboud University Nijmegen Medical Centre, PO Box 9101, 6500HB Nijmegen, The Netherlands

*Author for correspondence (e-mail: C.Figdor@ncmls.ru.nl)
‡Present address: Department of Radiology (667), Radboud University Nijmegen Medical Centre, PO Box 9101, 6500HB Nijmegen, The Netherlands

Accepted 3 September 2007
Journal of Cell Science 120, 3965-3976 Published by The Company of Biologists 2007
doi:10.1242/jcs.004010

Summary

The activated leukocyte cell adhesion molecule (ALCAM) mediates dynamic homotypic and heterotypic cellular interactions. Whereas homotypic ALCAM-ALCAM interactions have been implicated in the development and maintenance of tissue architecture and tumor progression, heterotypic ALCAM-CD6 interactions act to initiate and stabilize T-cell–dendritic-cell interactions affecting T-cell activation. The ability to resist the forces acting on the individual bonds during these highly dynamic cellular contacts is thought to be crucial for the (patho)physiology of ALCAM-mediated cell adhesion. Here, we used atomic force microscopy to characterize the relationship between affinity, avidity and the stability of ALCAM-mediated interactions under external loading, at the single-molecule level. Disruption of the actin cytoskeleton resulted in enhanced ALCAM binding avidity, without affecting the tensile strength of the individual bonds. Force spectroscopy revealed that the ALCAM-CD6 bond displayed a significantly higher tensile strength, a smaller reactive compliance and an up to 100-fold lower dissociation rate in the physiological force window in comparison to the homotypic interaction. These results indicate that homotypic and heterotypic ALCAM-mediated adhesion are governed by significantly distinct kinetic and mechanical properties, providing novel insight into the role of ALCAM during highly dynamic cellular interactions.

Supplementary material available online at
http://jcs.biologists.org/cgi/content/full/120/22/3965/DC1

Key words: ALCAM, CD166, CD6, Cytoskeleton, Force spectroscopy, AFM

Introduction

Cell adhesion molecules mediate cell attachment and play an important role in maintaining tissue organization by facilitating tissue development, transmembrane signaling and cell motility. Four major superfamilies of cell adhesion molecules have been identified so far: cadherin, selectin, integrin and the immunoglobulin superfamily. Overall cell adhesive properties are tightly regulated and crucially depend on the relative expression levels, molecular conformation (affinity) and on the local molecular density (valency) of adhesion receptors in the cell membrane (van Kooyk and Figdor, 2000; Carman and Springer, 2003; Cambi et al., 2004; Kim et al., 2004; Cambi et al., 2006). The tumorigenic and metastatic phenotype of various cancers are often correlated with altered relative expression levels of these molecules (Hanahan and Weinberg, 2000; Li, G. et al., 2003). In particular, the association between invasive growth of epithelial carcinomas, the loss of functional E-cadherin and the simultaneous expression of inappropriate cadherins is well documented (Hazan et al., 2004; Cowin et al., 2005; Knudsen and Wheelock, 2005). Whereas it is well known that the release from the primary tumor usually is accompanied by a loss of homotypic cell adhesion, it is also clear that considerable mechanical stresses are imposed on the membranes of cells and their associated adhesion molecules, while the cells migrate and reversibly attach to other cells and the extracellular matrix. How the mechanical properties of the different adhesion receptor pairs govern the distinct migratory phenotypes of tumor cells is not well understood.

In addition to changes in cadherin expression, other adhesion molecules have been implicated in the phenotypic switch associated with enhanced tumor invasiveness. The activated leukocyte cell adhesion molecule (ALCAM, CD166) is a member of the immunoglobulin superfamily of cell adhesion molecules (Ig-CAMs) (Bowen et al., 1995). Similar to some other members of this family (e.g. NCAM, CEA), ALCAM mediates homotypic ALCAM-ALCAM adhesion (Bowen et al., 1995; Nelissen et al., 2000; Zimmerman et al., 2004), but heterotypic interactions with the T-cell antigen CD6 have also been described (Bowen et al., 1995; Hassan et al.,

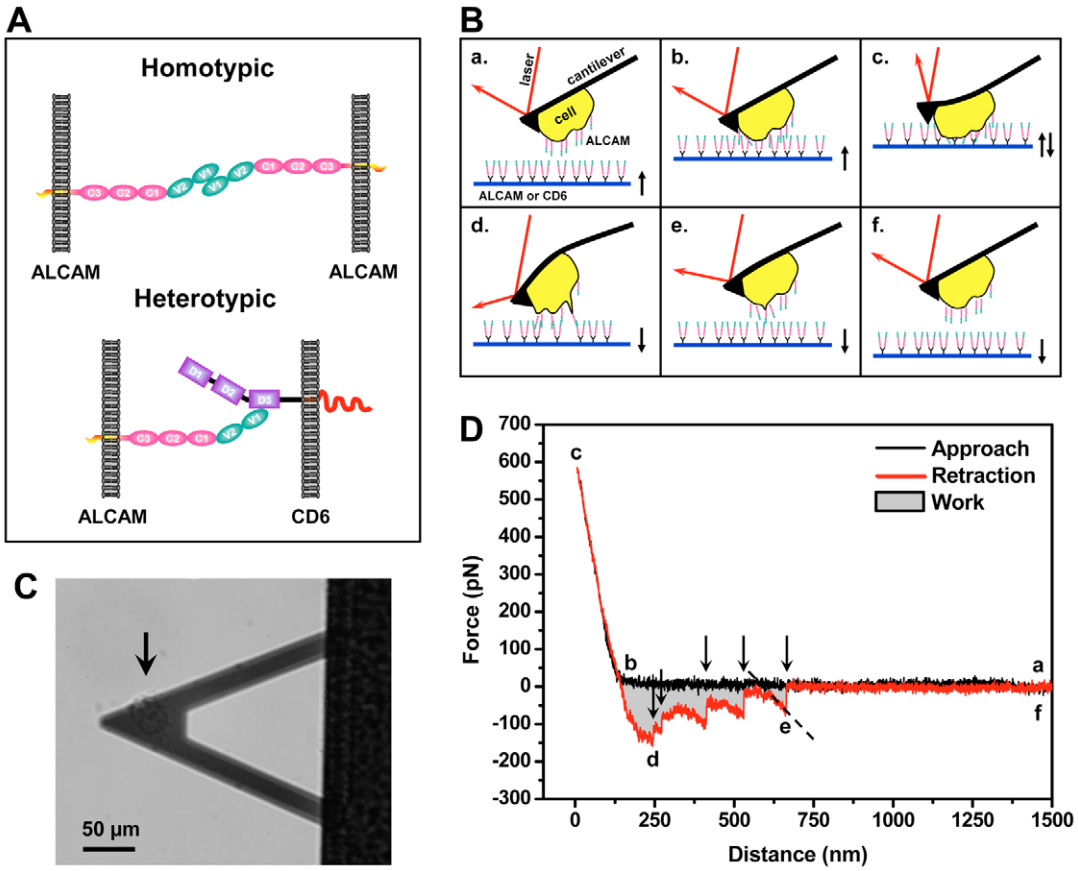

Fig. 1. ALCAM-mediated adhesion probed by AFM. (A) Homo- and heterotypic ALCAM-mediated interactions. ALCAM contains five Ig domains and the membrane-distal V1 Ig domain mediates homotypic ALCAM-ALCAM interactions (van Kempen et al., 2001). Heterotypic interactions to CD6, a member of the scavenger receptor cysteine rich (SRCR) protein family, are mediated by the ALCAM V1 Ig domain and the third, membrane-proximal, SRCR domain (D3) of CD6 (Bowen et al., 2000). (B) Schematic layout of the AFM experiment. Cells were attached to the AFM cantilever by a ConA-mediated linkage, as detailed in the Materials and Methods. An ALCAM-expressing cell attached to the AFM cantilever interacts with a substrate coated with either ALCAM-Fc or CD6-Fc under the control of the AFM. First (a) the substrate is moved to the cantilever by the piezoelectric scanner until contact is made (b). Then the substrate is pressed onto the cell, causing the cantilever to bend, until a specified force limit is reached. During a preset period of time (interaction time) the cell and substrate are allowed to interact (c). Upon retraction, the cell-substrate adhesion will cause the cantilever to bend in the other direction (d), until the force acting on the molecular bonds are large enough for bond rupture to occur (e). Finally, the cantilever returns to its resting position (f). (C) Example of a single K562-ALCAM cell (arrow), just visible in the shadow of the cantilever, attached to the end of the AFM probe. (D) A typical force-distance curve of an ALCAM-ALCAM interaction, showing single bond ruptures (arrows; K562-ALCAM on ALCAM-coated substrate). a-f correspond to those in B. From the slope just before the final rupture (broken line), the loading rate acting on the bond is calculated. The area enclosed by the approach and retraction curve (shaded) is a measure for the work of de-adhesion under these conditions.

2004) (Fig. 1A). Bone marrow stromal cells and hematopoietic progenitor cells, neuronal cells, and a large number of epithelial and endothelial cell types express significant levels of ALCAM, and contributions for homotypic ALCAM-mediated adhesion have been described for neural development, hematopoietic stem cell maturation and transendothelial monocyte migration (Tanaka et al., 1991; Patel et al., 1995; Degen et al., 1998; Swart, 2002; Masedunskas et al., 2006). ALCAM has been implicated in the onset and progression of melanoma (van Kempen et al., 2000; van Kempen et al., 2001; Lunter et al., 2005), bladder cancer (Tomita et al., 2003), prostate carcinoma (Kristiansen et al., 2003), breast cancer (King et al., 2004) and colorectal carcinoma (Weichert et al., 2004). The invasiveness of malignant melanoma correlates with enhanced ALCAM expression and this molecule is considered to be a prognostic marker in this disease (Degen et al., 1998; van Kempen et al., 2000; van Kempen et al., 2001; Swart et al., 2005).

Besides mediating homotypic interactions, ALCAM is the only known ligand for CD6 identified on immune cells. Recent work indicates that ALCAM localizes to the immunological synapse (Grakoui et al., 1999) in an antigen-dependent manner (Gimferrer et al., 2004) and that ALCAM-CD6 engagement plays a pivotal role both during early T-cell–dendritic-cell (DC) contact formation and in later stages of T-cell activation (Zimmerman et al., 2006). In fact, several studies now point towards a role for CD6 as a co-stimulatory molecule in T-cell activation (Gangemi et al., 1989; Wee et al., 1993; Rasmussen et al., 1994; Osorio et al., 1998; Hassan et al., 2004; Zimmerman et al., 2006). Recent intravital microscopy studies indicate that, within lymphoid tissue, naïve T cells scan the surface of DCs at relative cell speeds of up to 30 μm/minute

(Mempel et al., 2004). Clearly, the ability to withstand shear at the molecular level is essential for establishing and maintaining productive DC–T-cell contacts for prolonged periods of time.

These findings indicate a key role for ALCAM-mediated adhesion during highly dynamic cellular interactions. Mechanistically, this implies that ALCAM must be equipped to facilitate adhesion under different conditions of external loading. Previous work has focused on the affinity and avidity of ALCAM-mediated interactions (Nelissen et al., 2000; Hassan et al., 2004; Zimmerman et al., 2004). Yet, how these properties relate to the stability of ALCAM-mediated bonds under mechanical stress is still poorly understood. Here, we address this issue using the atomic force microscope (AFM) (Binnig et al., 1986) to measure ALCAM-mediated adhesion of living cells under varying loading conditions and with single-bond sensitivity. The AFM has been used successfully to study single-molecule adhesion of isolated proteins (Willemsen et al., 2000; Hinterdorfer, 2002), and later in studies towards cell adhesion phenomena – an approach that was first explored by Gaub and co-workers (Benoit et al., 2000). The use of force spectroscopy has meanwhile provided insight into the compliance of individual cell adhesion bonds to physiological-range external forces (Zhang et al., 2002; Wojcikiewicz et al., 2003; Hanley et al., 2004; Hinterdorfer and Dufrêne, 2006; Panorchan et al., 2006b).

We have adapted the AFM technology to study the stability of homo- and heterotypic ALCAM-mediated adhesion under loading. In the low-force regime the ALCAM-mediated interactions displayed similar dissociation kinetics. However, by applying physiologically relevant external forces we found that homo- and heterotypic ALCAM-mediated adhesion are governed by distinct kinetic and mechanical properties indicating that the ALCAM-CD6 bond is significantly more stable under mechanical stress. The reactive compliance and dissociation kinetics found for the ALCAM-CD6 interaction were similar in magnitude to those reported for selectin mediated bonds (Zhang et al., 2004b). By contrast, the ALCAM-ALCAM bond displayed a significantly greater lability under force, also in comparison to homotypic E-cadherin-mediated interactions (Panorchan et al., 2006b).

Results

Using AFM to measure single ALCAM-mediated interactions on living cells

A schematic layout of the AFM adhesion measurements is depicted in Fig. 1B. Cell adhesion forces were measured by moving ALCAM- or CD6-coated substrates alternately towards and away from an AFM cantilever to which a single ALCAM-expressing cell was attached by means of concanavalin A (ConA)-mediated linkages (Fig. 1B,C; see Materials and Methods). The detachment of the cell was recorded during retraction of the substrate. The rupture of cell-substrate bonds caused subtle changes in cantilever deflection that provided a measure for the cell adhesion forces that were acting on the molecular level (Fig. 1D, arrows). The work needed to detach the cell from the substrate – derived from the area enclosed by the retraction curve and the zero-force axis – was taken as a measure for overall cell adhesion (Zhang et al., 2002). Homo- and heterotypic ALCAM-mediated adhesions were compared using the same cell and cantilever probing the distinct ligand-coated substrates.

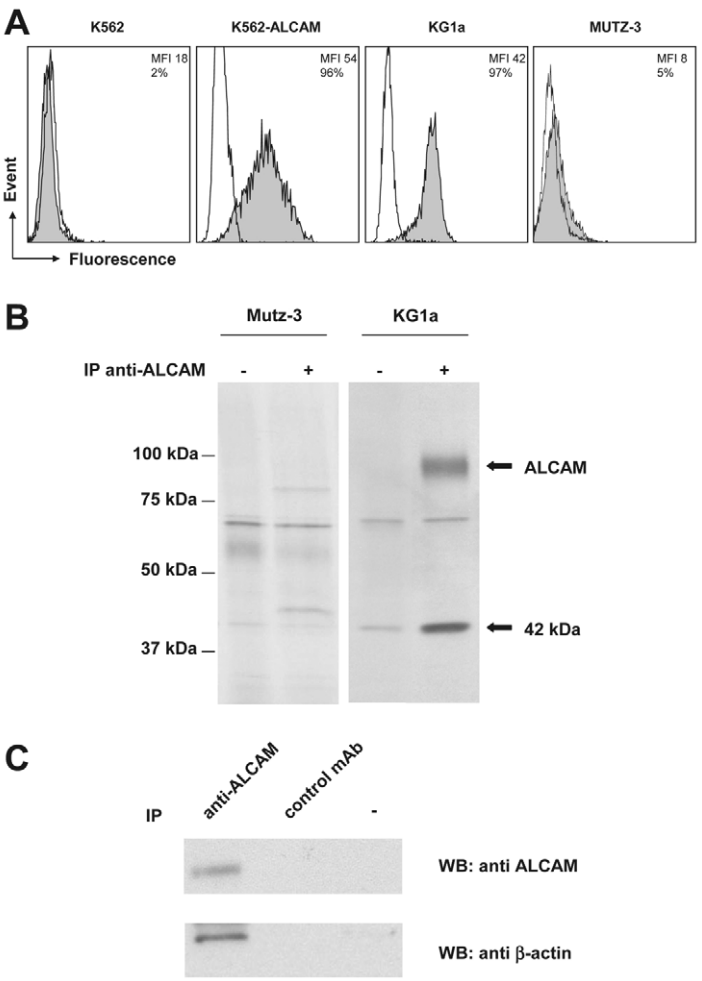

Fig. 2. ALCAM is associated with the actin cytoskeleton. (A) Surface expression of ALCAM on K562, K562-ALCAM, KG1a and undifferentiated MUTZ-3 cells was analyzed by flow cytometry. Unfilled histograms represent isotype control staining and shaded histograms represent staining with ALCAM antibody, AZN-L50. The mean fluorescence intensity (MFI) and percentage of positive cells are as indicated. (B) A 42 kDa protein co-precipitates with ALCAM from KG1a cells, as indicated by the arrows. KG1a and undifferentiated Mutz-3 control cells (no ALCAM expression) were incubated overnight with [^{35}S]methionine/cysteine. ALCAM was immunoprecipitated from labeled cell lysates with 1 μg of AZN-L51. Samples that were incubated with protein G beads alone (–) are shown as negative controls. (C) Identification of the co-precipitated protein by western blot analysis. ALCAM was immunoprecipitated from labeled KG1a cell lysates with 1 μg of AZN-L51. ALCAM and β-actin were detected using antibodies AZN-L50 and anti-β-actin (clone AC-15), respectively. As a negative control, lysates were incubated with an irrelevant control antibody (anti-hemagglutinin, clone 12CA5) or with protein G beads alone (–).

ALCAM is linked to the actin cytoskeleton

KG1a and ALCAM-transfected K562 cells (K562-ALCAM) both express similar levels of ALCAM at the cell surface (Fig. 2A). Parental ALCAM-negative K562 and MUTZ-3 cells were used as negative controls in further experiments. We found that a 42 kDa protein co-precipitates with ALCAM from metabolically labeled KG1a cells, but not from ALCAM-negative MUTZ-3 cells (Fig. 2B). This 42 kDa protein was identified as β-actin by immunoprecipitation (IP) of ALCAM followed by western blot analysis (Fig. 2C). Total cell lysate served as a control for total amounts of ALCAM and β-actin (not shown). Control IPs with either protein G beads alone or with a control antibody were negative for both ALCAM and β-actin, confirming the specificity of the interaction. These results confirm and extend our previously reported finding that ALCAM-mediated adhesion is directly regulated by the actin cytoskeleton (Nelissen et al., 2000; Zimmerman et al., 2004).

Avidity of ALCAM-mediated adhesion is controlled by the actin cytoskeleton

We have previously shown by means of an optical-trap-based motility assay and fluorescence microscopy that modest disruption of the cortical actin cytoskeleton – using cytochalasin D (CytD) – results in enhanced lateral mobility of ALCAM and the formation of ALCAM clusters on the cell surface. Interestingly, CytD pretreatment further enhanced cell adhesiveness to ALCAM–Fc-coated plates, suggesting that the observed clustering effectively enhanced ALCAM binding avidity (Nelissen et al., 2000; Zimmerman et al., 2004). Here, we exploit the sensitivity of the AFM to determine to what extent the affinity of individual ALCAM-mediated interactions contributes to this effect.

Fig. 3A shows the effect of CytD on the work (shaded area) needed to detach a KG1a cell from an ALCAM–Fc-coated plate. For clarity, the traces are shown with an offset. After the initial acquisition of force-distance curves, the cell was stimulated in situ with CytD and re-examined under identical experimental conditions. Subsequently, ALCAM-mediated adhesion was blocked using mAb AZN-L50. Similar experiments were performed to study the adhesion to CD6–Fc-coated plates (curves not shown). The effect of CytD was most pronounced in the case of the homotypic interactions (Fig. 3B). We found that CytD treatment caused an up to twofold enhancement in overall cell adhesion. Subsequent incubation with mAb AZN-L50 blocked ~80% of total adhesion (i.e. back to the level of untreated cell adhesion in the presence of this antibody), indicating that the CytD-enhanced adhesion was ALCAM specific. Similar results were obtained on CD6–Fc-coated plates, albeit that the enhancement in adhesion and subsequent blocking was slightly less pronounced. Overall, these results are in excellent agreement with our previous findings using a plate adhesion assay (Nelissen et al., 2000; Zimmerman et al., 2004).

The ability of the AFM to measure binding forces on the molecular scale prompted us to re-examine whether CytD might also affect the affinity of the homo- and heterotypic interactions. Affinity changes are expected to result in concomitant changes in rupture force (Zhang et al., 2002; Wojcikiewicz et al., 2003). Rupture forces were determined from the final rupture events, before and after CytD or AZN-L50 treatment. However, in contrast to the effects on overall cell adhesion described above, the mean rupture forces for the homo- and heterotypic

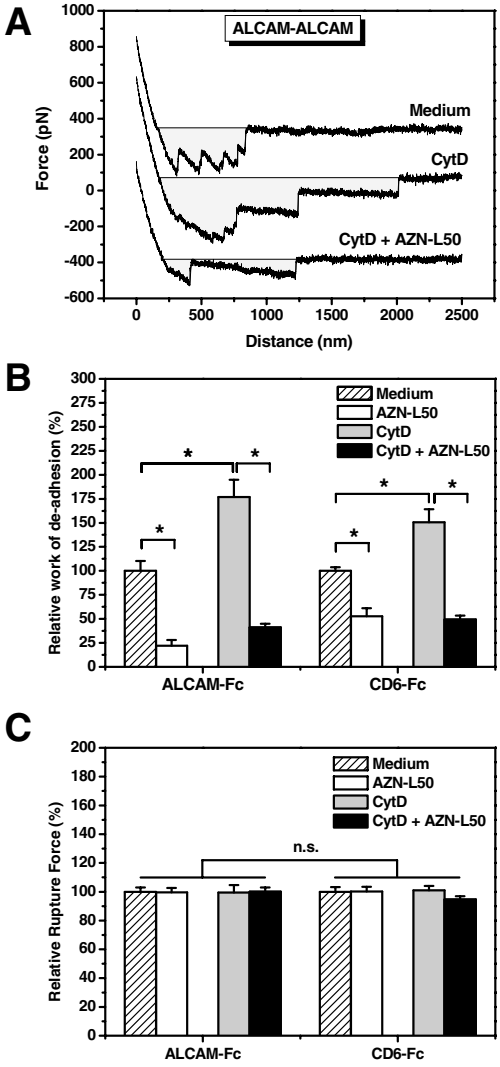

Fig. 3. The actin cytoskeleton regulates ALCAM binding avidity. (A) Typical force-distance curves of the homotypic ALCAM-mediated interaction between a KG1a cell and an ALCAM–Fc-coated plate, before (medium) and after treatment with the actin cytoskeleton inhibitor CytD, and after a subsequent blocking step (CytD + mAb AZN-L50). For clarity, the traces are shown with an offset. The substrate retraction speed was set to 2.5 μm/second. The work needed to detach the cell from the substrate (shaded areas), typically between 1×10^{-16} and 3×10^{-16} J for untreated cells, was taken as a measure for overall cell adhesion. (B) Whole-cell analyses of the relative work of de-adhesion comparing the situation before treatment (medium) with that after incubation with the ALCAM-function-blocking mAb AZN-L50, or after incubation with CytD alone and followed by a subsequent AZN-L50 incubation. The relative work of de-adhesion was determined from at least 25 traces per cell per condition (medium condition set to 100%). It can be seen that CytD treatment upregulates overall cell adhesion and that this adhesion is ALCAM-specific. (C) Single-bond-level rupture-force analyses. In contrast to the overall cell adhesion, the single-bond rupture forces under these loading conditions were found to be insensitive to the various treatments (relative force-scale; $n>30$). Error bars represent s.e.m.; * indicates significance to $P<0.05$; n.s., not significant. Trends were reproducibly observed in three independent experiments.

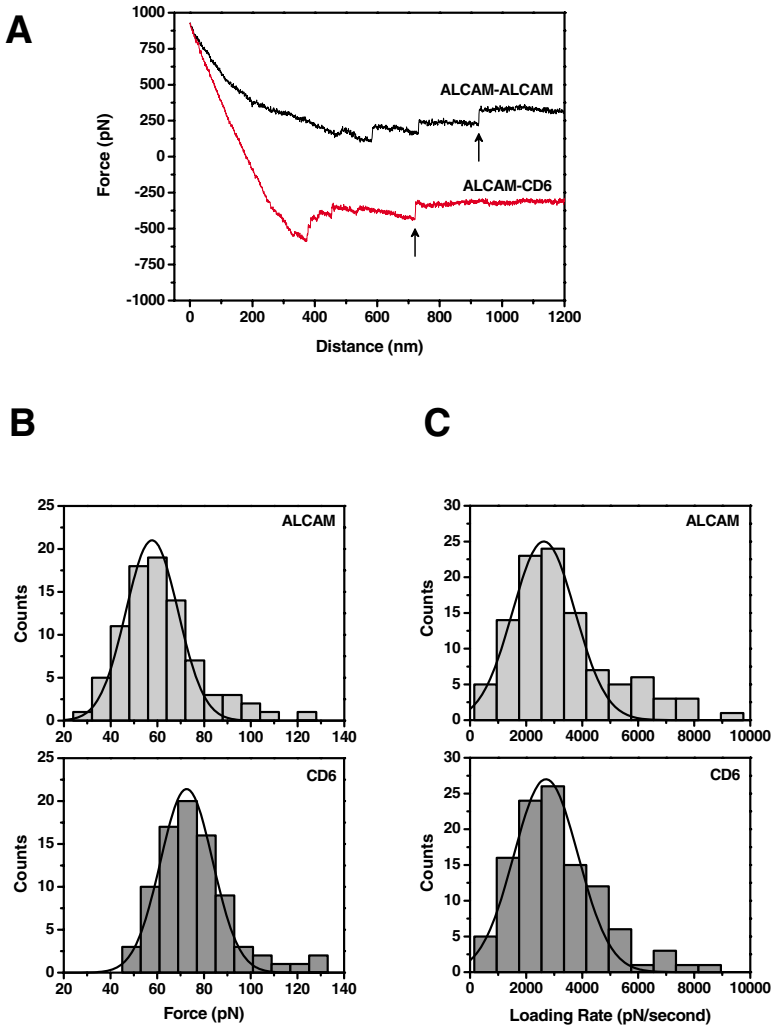

Fig. 4. Single-molecule force measurements on living KG1a cells. (A) Examples of force-distance curves obtained in the low-adhesion regime (~50×10^{-18} J, see text). Final ruptures (arrows) were used for further analyses. The retraction speed was set to 2.5 μm/second. (B) Statistical analysis of the rupture forces. The mean rupture forces (± s.e.m.) determined from these data were 58±3 pN and 73±3 pN for the ALCAM-ALCAM and ALCAM-CD6 bond, respectively (P<0.001, n=85; see also Fig. 5). (C) Statistical analysis of the loading rates. The mean loading rates were found to be similar in magnitude (i.e. 2632±112 pN/second and 2707±115 pN/second for the homo- and heterotypic bonds, respectively) (n>100; not significant). A single Gaussian function (solid lines) could be fitted to the force- and loading-rate distributions, which, in all cases, accounted for >85% of the events.

interactions were not affected by either treatment (Fig. 3C). These results clearly demonstrate that disruption of the actin cytoskeleton by CytD enhances ALCAM binding avidity without affecting the affinity of the individual ALCAM-mediated interactions.

The ALCAM-CD6 bond is more stable under external loading

Previous work focused on the affinity of ALCAM-mediated interactions using soluble ligand binding assays (Hassan et al., 2004; Zimmerman et al., 2004). Here, we address the relative stability of single homo- versus heterotypic ALCAM-mediated bonds under conditions of external loading (i.e. under conditions that mimic the forces acting on the cell adhesion molecules during dynamic cell-cell contacts).

To compare cell adhesion to different substrates, interaction times were adjusted to control the overall level of adhesion. The extent of adhesion between cell and substrate depended both on the interaction time and the force exerted on the cell during that time. Moreover, local variations in receptor density were anticipated to affect adhesion. It has been shown that short interaction times promote the detection of single-bond ruptures as opposed to the simultaneous rupture of multiple bonds (Benoit et al., 2000; Hanley et al., 2003; Li, F. et al., 2003; Hanley et al., 2004). Control experiments were performed to determine the threshold level of adhesion in this assay. When a parental K562 cell – not expressing ALCAM – was lowered onto an ALCAM–Fc-coated substrate, or even an uncoated, substrate, non-specific adhesion sometimes occurred (data not shown). However, although these events could not be distinguished from specific ruptures on the basis of rupture force alone (not shown), the apparent work of de-adhesion associated with these non-specific events was small, typically $\leqslant20\times10^{-18}$ J. Therefore, to further promote the capture of specific single-bond ruptures, interaction times were adjusted to obtain a detachment work of ~50×10^{-18} J, sufficient to allow for a clearly visible block with the mAb AZN-L50. Typical force-distance curves acquired in this way are presented in Fig. 4A, and are again offset for clarity. To further reduce the chance of measuring multiple bond ruptures, only the final events (Fig. 4A, arrows) were used to extract the rupture-force and loading-rate data (Wong et al., 1999). Fig. 4B,C show the statistical analysis compiled from more than 100 of these curves taken at a fixed substrate retraction speed. The rupture force (Fig. 4B) and loading rate (Fig. 4C) distributions could be fitted to a single Gaussian function, which, in all cases, accounted for over 85% of the events. We note that multiple bond ruptures would have resulted in multiple quantized peaks (Wong et al., 1999; Benoit et al., 2000). Taken together, by performing the experiments under conditions of moderate adhesion, we found that over 85% of the events included in this assay represented single ALCAM-mediated bond ruptures.

When both homo- and heterotypic ALCAM-mediated bonds were loaded at a similar rate of 2700 pN/second (Fig. 4C), the mean rupture force determined for the ALCAM-CD6 bond was 73±3 pN, significantly higher than the 58±3 pN found for the homotypic interaction (± s.e.m., P<0.001; Fig. 4B). These data show that, relative to the homotypic interaction, the ALCAM-CD6 bond can resist higher forces, indicating that this bond will be the more stable under conditions of dynamic cell-cell interactions.

Distinct mechanical properties govern homo- and heterotypic ALCAM-mediated interactions

Force spectroscopy was applied to characterize and compare the biochemical and biophysical properties underlying the

stability of individual ALCAM-mediated interactions under conditions of varying mechanical stress. Force spectra were obtained by examining the mean rupture forces determined as described above, but now for loading rates varying in the range from 300 to 20,000 pN/second – mimicking cell-cell speeds ranging from 0.2 to 13.0 μm/second. Experiments were performed using both KG1a and K562-ALCAM cells, and the resulting force spectra are displayed in Fig. 5A. Importantly, the similarity of the force spectra obtained from both cell types further substantiates the conclusion that exclusively ALCAM-mediated bond ruptures were probed.

The mean rupture forces found for both the homo- and heterotypic interactions increase linearly as a function of the natural logarithm of the loading rate. This behavior was first described by Bell (Bell, 1978). In the Bell model, the mean rupture force F_{rup} is described by:

$$F_{rup} = \frac{k_B T}{x_\beta} \ln\left(\frac{x_\beta}{k_{off}^0 k_B T}\right) + \frac{k_B T}{x_\beta} \ln(r_f), \quad (1)$$

where k_{off}^0 is the (unstressed) dissociation rate in the absence of a pulling force; x_β is the reactive compliance or mechanical bond-length; T is the absolute temperature; k_B is the Boltzmann constant; and r_f is the loading rate (Evans and Ritchie, 1997; Alon et al., 1998; Tees et al., 2001; Hanley et al., 2003). The Bell model parameters k_{off}^0 and x_β, characterizing the micromechanical properties of the homo- and heterotypic ALCAM-mediated interactions, were obtained by fitting the spectra to Eqn 1. Table 1 lists these parameters, and shows a comparison to other receptor-ligand pairs to put the ALCAM data into perspective (see Discussion). The data did not show a significant difference in unstressed dissociation rates – 1.9 versus 3.4 second^{-1} for the homotypic and heterotypic bond, respectively. By contrast, the mechanical bond length determined for the ALCAM-CD6 interaction was 0.23±0.01 nm, significantly shorter than the 0.38±0.06 nm we found for the ALCAM-ALCAM bond. Because these numbers are in the range of the bond lengths of a single Van der Waals interaction or hydrogen bond, the observed differences in mechanical bond length probably reflect distinct (hydrogen) bonding patterns in

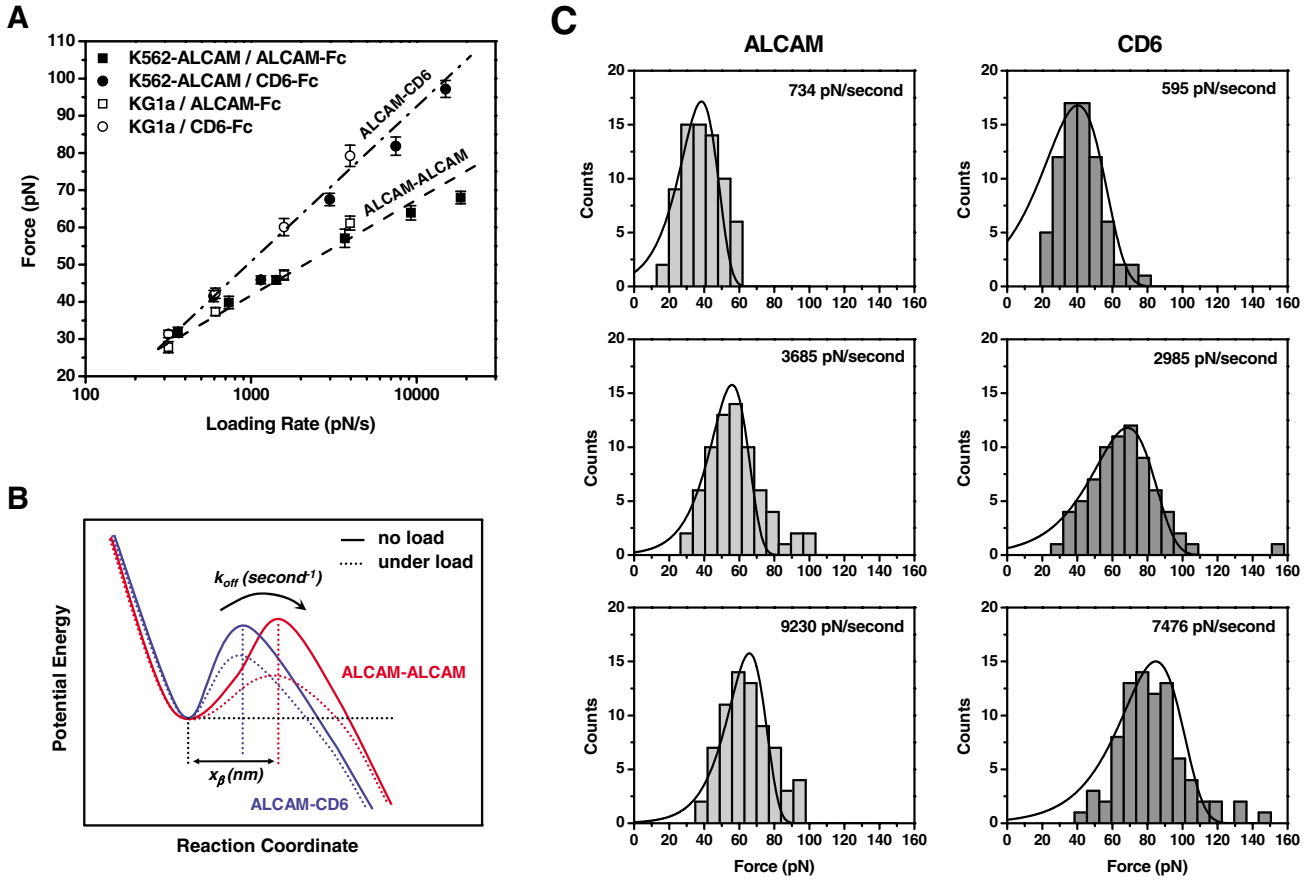

Fig. 5. Force spectra of ALCAM-mediated interactions. (A) The mean rupture forces for the homotypic (circle) and heterotypic (square) ALCAM-mediated interactions were found to increase linearly with the natural logarithm of the loading rate. This behavior is consistent with the Bell model (see text, R^2>0.95). The results obtained using KG1a (white symbol) were similar to those using K562-ALCAM cells (black). At loading rates >1500 pN/second, the forces associated with ALCAM-CD6 bond rupture were significantly higher than those for the ALCAM-ALCAM interaction (n>20, P<0.05; error bars indicate s.e.m.). (B) Schematic representation of the significance of the Bell model parameters in terms of the energy barrier between the bound and unbound state. The situation when no force is applied (solid lines) or when external forces are applied to the bonds (dotted lines, see Discussion) is represented. (C) Comparison of the histograms of rupture forces (K562-ALCAM cells, n>70; three loading rates) and the theoretical probability density distributions for the failure of single ALCAM-ALCAM and ALCAM-CD6 bonds.

Table 1. The kinetics and reactive compliance of ALCAM-mediated interactions placed in context

System	$x_{\beta 1}$ (nm)	k_1^0 (second^{-1})	$x_{\beta 2}$ (nm)	k_2^0 (second^{-1})	Reference
ALCAM-ALCAM[a]	0.38±0.06*	1.9±0.8*			This work
ALCAM -CD6[a]	0.23±0.01*	3.4±0.3*			This work
N-cadherin–N-cadherin[b]	0.77±0.09	0.98±0.46			(Panorchan et al., 2006b)
E-cadherin–E-cadherin[c]	0.32±0.07	1.09±0.35	0.10±0.02	4.00±0.68	(Panorchan et al., 2006b)
VE-cadherin–VE-cadherin[b]	0.42±0.03	0.45±0.12			(Panorchan et al., 2006a)
P-selectin–PSGL-1[d]	0.15±0.01	0.22±0.06			(Hanley et al., 2004)
LFA-1–ICAM-1 (low affinity)[e]	0.15	4.0	0.018	57	(Zhang et al., 2002)
LFA-1–ICAM-1 (high affinity)[e]	0.21	0.17	0.024	40	(Zhang et al., 2002)
E-selectin–sLeX[f]	0.5	0.3	0.09	65	(Zhang et al., 2004a)

[a]Loading rate 300-20,000 pN/second; [b]loading rate 50-5000 pN/second; [c]loading rate 100-500 pN/second (lower regime), 500-10,000 pN/second (higher regime); [d]loading rate 100-10,000 pN/second; [e]loading rate 20-10,000 pN/second (lower regime), 10,000-50,000 pN/second (higher regime); [f]loading rate 100-10,000 pN/second (lower regime), 10,000-100,000 pN/second (higher regime).

*Error estimation on the basis of a comparison between the data derived from both cell types.

both types of ALCAM-mediated interactions (Fig. 1A). Bonds with shorter x_β are more resistant to applied force. These findings, therefore, corroborate the previous conclusion that, with respect to the homotypic interaction, the ALCAM-CD6 bond is more resistant to applied force, and hence more stable under loading than the ALCAM-ALCAM bond.

In terms of interaction potentials, the unstressed dissociation rate k_{off}^0 represents the rate-limiting step in the dissociation (i.e. the transition over the activation barrier) of the unstressed complex. The reactive compliance, x_β, then represents the reaction coordinate, and describes how far the bond can be stretched before it breaks (Hummer and Szabo, 2001; Rief and Grubmüller, 2002). A schematic graphical representation of the data is shown in Fig. 5B (solid curves). The linearity of the force spectra (Fig. 5A) indicates that, in this loading-rate regime, the dissociation of ALCAM-mediated interactions is best described by a single activation energy barrier. By contrast, bi-phasic force spectra reflecting a double-barrier interaction potential have been reported [e.g. for E-cadherin–E-cadherin, LFA-1–ICAM-1, and E-, P- or L-selectin–sLex (sialyl Lewis X) (Evans et al., 2001; Zhang et al., 2002; Zhang et al., 2004a; Panorchan et al., 2006b)]. The Bell model predicts that, with increasing loading forces, the activation energy barrier of the complex is suppressed and the dissociation rate constant increases. This is shown schematically in Fig. 5B and is discussed below.

Fig. 5C shows a comparison of the histograms of rupture forces at three loading rates and the corresponding probability density distributions for the failure of single ALCAM-ALCAM and ALCAM-CD6 bonds that were calculated using the Bell model parameters derived from Fig. 5A using (Evans and Ritchie, 1997; Li, F. et al., 2003):

$$P(F_{rup}) = k_{off}^0 \exp\left(\frac{x_\beta F_{rup}}{k_B T}\right) \exp\left\{\frac{k_{off}^0 k_B T}{x_\beta r_f}\left[1 - \exp\left(\frac{x_\beta F_{rup}}{k_B T}\right)\right]\right\}. \quad (2)$$

As can be seen in Fig. 5C, the theoretical distributions closely match the histograms of rupture forces at all three loading rates. The width of the distributions does not reflect experimental error, but is a manifestation of the underlying stochastic distribution of breakup times (Evans and Ritchie, 1997; Tees et al., 2001; Evans et al., 2005). The small number of events beyond the predicted distributions, <16% of events in all cases in Fig. 5C, can be accounted for by the simultaneous (i.e. unresolved) rupture of multiple bond linkages (Evans et al., 2005). Importantly, this analysis implies that indeed ~85% of the events represent the kinetically limited failure of single bonds.

Control experiments were performed to verify whether the attachment of the cells to the cantilevers by means of ConA-mediated linkages possibly activated the cells and affected the outcome of the single-molecule adhesion measurements. K562-ALCAM cells were seeded onto poly-L-lysine-coated glass coverslips and probed with a 10 μm ALCAM–Fc- or CD6–Fc-coated bead glued to an AFM cantilever (see supplementary material Fig. S1A). The interactions were found to be ALCAM-specific and showed a clear single-molecule signature (see supplementary material Fig. S1B,C). The mean rupture forces for both the homo- and heterotypic ALCAM-mediated interactions that were found under varying pulling conditions agree well with the data obtained using the cell-functionalized cantilevers (supplementary material Fig. S1D). These data show that the presented single-molecule-level adhesion measurements are independent of the probing method.

Finally, the dissociation energies of single ALCAM-mediated interactions were derived from the net amount of work required to break the bonds, by calculating the product of rupture force and rupture length. The work to break a single ALCAM-ALCAM interaction – at 1000 pN/second, corresponding to a pulling speed of 700 nm/second – amounted to 40 pN ×0.38 nm ≈ 4 k_BT (Fig. 5A; T=300 K). Interestingly, under the same conditions, due to the higher unbinding force and the shorter reactive compliance, the net work to rupture an ALCAM-CD6 bond was 50 pN ×0.23 nm ≈ 3 k_BT. Hence, despite the shorter mechanical bond length, under physiologically relevant loading we found that the net work to break a single ALCAM-CD6 interaction was similar in magnitude to that found for the dissociation of the ALCAM-ALCAM complex. We note that, in order to extract a transmembrane protein from the cell membrane, around 70 kcal/mol is required (Chen and Moy, 2000) (i.e. about ~120 k_BT for a single protein). Previous reports suggested that Ig-CAMs might cushion shear stresses at cell-cell contacts in the immune system by forced (reversible) unfolding of their Ig domains (Carl et al., 2001; Bhasin et al., 2004). However,

under similar loading conditions, these authors reported the net work to unfold an Ig domain to be in the 13-16 k_BT regime (Carl et al., 2001). Therefore, rather than inducing unfolding of the ALCAM Ig domains, we believe that shear-related loading of ALCAM-mediated bonds in vivo will result in bond rupture, as suggested here.

In summary, we found that the dissociation of homo- and heterotypic ALCAM-mediated interactions are governed by distinct mechanical properties, revealing the molecular basis for the higher relative stability of the ALCAM-CD6 bond than the ALCAM-ALCAM bond under external loading.

Discussion

ALCAM mediates cell adhesion during highly dynamic cellular interactions and hence under varying conditions of external loading. The relationship between the affinity and avidity of ALCAM-mediated interactions, and the ability of this molecule to facilitate productive cellular interactions under mechanical stress is poorly understood. We applied force spectroscopy to study the relative stability of single homo- and heterotypic ALCAM-mediated interactions on living cells and in a dynamic setting mimicking cell-cell interactions at relative speeds ranging from 0.2 to 13.0 μm/second.

Previous reports indicated that ALCAM-mediated adhesion of K562-ALCAM cells is dynamically regulated through the actin cytoskeleton. Treatment of the cells with agents that disrupt the cortical cytoskeleton [e.g. the actin polymerization inhibitor cytochalasin D (CytD) or latrunculin A] significantly enhanced adhesion to ligand-coated plates (Nelissen et al., 2000; Zimmerman et al., 2004). Here, we provide biochemical evidence that ALCAM can associate with β-actin. We further show, by means of single-molecule resolution adhesion measurements, that, although CytD treatment indeed enhances overall cell adhesion, it does not affect the tensile strength of the individual bonds. This unequivocally demonstrates that CytD affects ALCAM binding avidity rather than its affinity. Avidity enhancement could be due either to an enlarged cell-substrate contact area under force – facilitated by a possible loss of cortical tension – or enhanced microclustering of the more freely diffusing ALCAM molecules, as was suggested in the previous studies. Alternatively, avidity enhancement might occur through attenuated ALCAM-cytoskeleton interactions, influencing membrane separation from the cytoskeleton and hence the onset of tether formation (Evans et al., 2005). Membrane tethers were suggested to dampen the shear forces in flow-chamber assays, enabling a longer duration of receptor-ligand attachment and thereby affecting binding avidity (Evans et al., 2005). The exact cause of the avidity change is currently under investigation. By combining AFM with confocal fluorescence microscopy and using high-resolution whole-mount transmission electron microscopy (Cambi et al., 2004; Cambi et al., 2006), we are currently exploring how the actomyosin cytoskeleton regulates these avidity changes.

By performing the AFM experiments under well-defined conditions of moderate adhesion, we were able to assign the observed sudden force jumps to single ALCAM-specific unbinding events. Indeed, apart from the fact that adhesion could be blocked using the ALCAM function-blocking mAb AZN-L50, significantly different force spectra were obtained for the ALCAM-ALCAM and ALCAM-CD6 bonds. Furthermore, the force-spectra were found to be essentially independent of the cell-type studied. Interestingly, this also indicates that the local membrane environment and the overall cell viscoelastic properties do not significantly affect the outcome of the single-molecule adhesion measurements. This is consistent with literature data showing that force spectra could be reproduced even after cells were fixed (Tees et al., 2001; Li, F. et al., 2003; Hanley et al., 2004; Panorchan et al., 2006b). The present observation that, on living cells, CytD does not affect the ALCAM-specific unbinding forces validates and extends these findings.

The equilibrium parameters for the ALCAM-ALCAM and ALCAM-CD6 interactions have previously been derived from surface-plasmon-resonance experiments and indicated a tenfold difference in dissociation rate (i.e. 5 second^{-1} versus 0.5 second^{-1}, respectively) for the homo- and heterotypic interaction, and a 100-fold higher affinity (K_D) of ALCAM for CD6 (Hassan et al., 2004). Interestingly, the unstressed dissociation rates derived here (1.9 versus 3.4 second^{-1}, Table 1), although in overall agreement, do not show this relative difference. This is probably because of the fact that, in our case, the unstressed off-rates are derived by extrapolation from the higher loading regime. Here, the unbinding events might be forced through a specific pathway and hence might be expected to exhibit fewer degrees of freedom – a situation that is clearly distinct from that occurring in soluble ligand binding assays, and might be more physiological. By contrast, we found that the ALCAM-CD6 interaction displayed higher tensile strengths and a significantly smaller reactive compliance, suggesting that this bond will be more resistant to applied force, and hence more stable under conditions of mechanical stress.

The stability of the adhesive bonds can be quantified by the dissociation rates of the interactions under conditions of external loading. The Bell model predicts that, with increasing loading forces, the dissociation rate constants increase. The micromechanical properties derived here were used to compare the dissociation rates of the homo- and heterotypic ALCAM-mediated interactions under mechanical stress, and to place them in context. The force dependence of the dissociation rate of a bond displaying an inner and an outer activation barrier is given by:

$$k_{off} = 1 / [k_1^{0-1} \exp(-Fx_{\beta_1}/k_BT) + k_2^{0-1} \exp(-Fx_{\beta_2}/k_BT)] , \quad (3)$$

where the subscripts (1,2) indicate the outer and inner barrier, respectively (Evans et al., 2001). For ALCAM-mediated adhesion that only displayed a single activation barrier, the denominator contains a single term only. Fig. 6 shows a comparison, based on the data listed in Table 1, of the kinetic profiles of the ALCAM-ALCAM and ALCAM-CD6 bonds with those of P-selectin–PSGL-1 (Hanley et al., 2003; Hanley et al., 2004), E-selectin–sLeX (Zhang et al., 2004a), low- and high-affinity LFA-1–ICAM-1 (Zhang et al., 2002) and homotypic E-, N- and VE-cadherin interactions (Panorchan et al., 2006a; Panorchan et al., 2006b). Interestingly, although the dynamic force spectroscopy measurements did not show a significant difference in dissociation rates at low forces, with respect to the ALCAM-CD6 interaction a 10- to 100-fold higher lability for the homotypic ALCAM interaction is predicted in the 75-125 pN regime, probably representing the high-end of the physiologically relevant force range (Carl et

al., 2001; Li, F. et al., 2003). A schematic representation of this finding is presented in Fig. 5B (dotted curves).

Homotypic ALCAM-mediated interactions have been implicated in the onset of melanoma, because, besides the switching from E- to N- and VE-cadherin expression, ALCAM is also detected in early melanocytic transformation stages (reviewed by Swart et al., 2005). The ALCAM-positive metastatic phenotype of melanoma cells is characterized further by the absence of significant levels of the cadherins (Uhlenbrock et al., 2004; Swart et al., 2005). Fig. 6A compares the force-response curves of homotypic ALCAM-mediated and E-, N- and VE-cadherin-mediated interactions. Although the unstressed dissociation rates of these molecules are similar in magnitude, ALCAM and VE-cadherin display an up to three orders of magnitude higher dissociation rate in the physiological force-window, with respect to E-cadherin. For N-cadherin, this is already the case in the 30-40 pN range, and the relative lability of this bond under loading has been associated with the ability of breast tumor cells to break away from the primary tumor (Panorchan et al., 2006b). Similarly, expressing ALCAM rather than E-cadherin is anticipated to relieve the firm adhesive constraints facilitating transformed melanoma cells to escape the local tumor environment. The data further indicate that, under force, ALCAM will be able to sustain sufficient levels of adhesion. Hence, the kinetic and mechanical properties of the homotypic ALCAM-mediated interaction are consistent with a role for this bond in promoting the migratory phenotype of melanoma cells.

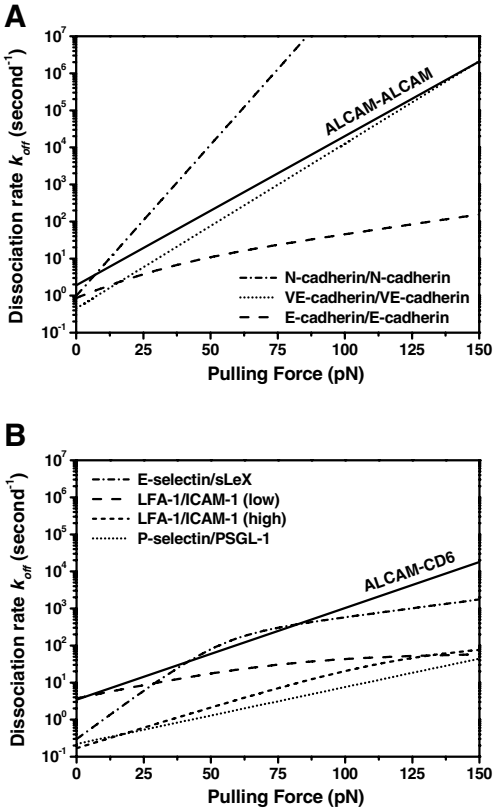

Fig. 6. Kinetic profiles of the ALCAM-mediated interactions placed in context. The kinetic profiles of ALCAM-mediated interactions, based on the derived Bell model parameters, are compared to (A) homotypic E-, N- and VE-cadherin-mediated interactions, and (B) LFA-1–ICAM-1 (low and high affinity), P-selectin–PSGL-1 and E-selectin–sLex interactions (see text).

The heterotypic ALCAM-CD6 interaction, in the 20–120 pN force window (Fig. 6B), compares well – kinetically – with the rolling receptor pair E-Selectin–sLeX (Zhang et al., 2004a). Besides its role in extravasation, E-selectin–sLeX interactions play a role in the vascular invasion and metastasis of human gallbladder adenocarcinoma (Kashiwagi et al., 2004). P-selectin–PSGL-1 and LFA-1–ICAM-1 are involved in leukocyte rolling and firm adhesion to vascular endothelium during inflammation, respectively. Clearly, high resistance to force is biologically important for the ability of these molecules to maintain cell-cell interactions in the blood flow. Consistent with their biological role, these receptor pairs show significantly smaller dissociation rates compared with the ALCAM-mediated interactions over the entire force-window. In DC–T-cell interactions, ALCAM and CD6 are rapidly recruited to the contact site in an antigen-dependent way, most probably under control of the actomyosin cytoskeleton (Gimferrer et al., 2005; Zimmerman et al., 2006), and the ALCAM-CD6 interaction reportedly has a dual function in that it both facilitates stable adhesion and provides a co-stimulatory signal (Zimmerman et al., 2006). The data presented here demonstrate that, in the dynamic environment of the lymph node, this interaction is indeed sturdy enough to play a significant role in establishing early DC–T-cell contact, in damping of shear stress and in providing long-term stabilization to the highly organized structure of the immunological synapse.

Taken together, the single-molecule-resolution adhesion measurements presented here have allowed us to obtain novel insight in the (patho)physiological role and regulation of ALCAM-mediated cell adhesion on a scale that was previously inaccessible. More generally, this work shows that measuring adhesion forces under external loading more accurately reflects differences between cell adhesion molecules that are not apparent in soluble ligand binding assays.

Materials and Methods

Chemicals and antibodies

Chemicals were purchased from Sigma (St Louis, MO) unless stated otherwise. The stock solution of CytD was prepared in dimethylsulfoxide (DMSO) and stored at –20°C. Anti-ALCAM monoclonal antibodies – AZN-L50 (IgG2A isotype) and AZN-L51 (IgG1 isotype) – were generated in our laboratory by immunizing BALB/C mice with K562-ALCAM. Goat-anti-human Fc-(Fab′)$_2$ fragments were purchased from Jackson ImmunoResearch (Westgrove, PA), FITC-conjugated goat-anti-mouse (Fab′)$_2$ fragments were purchased from Zymed Laboratories (San Francisco, CA). Recombinant ALCAM-Fc consisting of the extracellular domains of the ALCAM fused to the human IgG1 Fc tail was produced and purified as described elsewhere (Nelissen et al., 2000), and recombinant CD6-Fc was purchased from R&D Systems (Minneapolis, MN).

Cell lines and cultures

Culture media, serum and antibiotics were purchased from Gibco Invitrogen (Breda, The Netherlands). All culture media were supplemented with 1% antibiotics/antimycotics. Myelomonocytic KG1a cells were cultured in Iscove's modified Dulbecco's medium containing 10% FCS as described previously (Zimmerman et al., 2004). Erythroleukemic K562 cells were cultured in RPMI 1640 containing 10% FCS. K562-ALCAM cells were generated and maintained as described elsewhere (Nelissen et al., 2000). Human myeloid MUTZ-3 cells were cultured in 12-well plates in MEMα supplemented with ribonucleosides, desoxyribonucleosides, 20% FCS, 50 μM β-mercaptoethanol and 10% 5637 conditioned medium (Quentmeier et al., 1996; Kim et al., 2006).

Flow cytometry

Cells were washed with PBA [phosphate buffered saline (PBS) containing 1% (w/v)

bovine serum albumin (BSA) and 0.05% (w/v) NaN_3] and stained for 30 minutes at 4°C with AZN-L50 primary antibody (2-5 μg/ml in PBA). Cells were washed with PBA and incubated with FITC-conjugated goat-anti-mouse $(Fab')_2$ secondary antibodies. After washing, cells were analyzed on a FACScan analyzer (Becton Dickinson, Oxnard, CA). The gates were set to exclude dead cells and 5000 gated cells were analyzed. Data are displayed as histograms of fluorescence intensity versus cell count.

Radioactive cell labeling and immunoprecipitation

KG1a or control MUTZ-3 cells were pre-incubated for 1 hour in serum- and methionine/cysteine-free RPMI 1640 medium prior to labeling with Tran[^{35}S]-label (MP Biomedicals, Irvine, CA), 250 μCi per 10×10^6 cells for 16 hours at 37°C. Cells were washed once in PBS and subsequently lysed in lysis buffer A (50 mM Tris pH 7.5, 0.5% Triton X-100, 300 mM NaCl, 1.5 mM $MgCl_2$, 0.2 mM EDTA, 0.5 mM DTT, 1 mM PMSF, 1 μg/ml leupeptin and aprotinin). Lysates were subjected to immunoprecipitation with 1 μg of AZN-L51 antibody coupled to Protein G Sepharose 4 Fast Flow beads (Amersham Biosciences). Beads were washed three times in lysis buffer A and bound proteins were eluted by boiling in Laemmli sample buffer and subjected to 9% SDS-PAGE under reducing conditions. Radioactive proteins were detected by exposure to X-ray film (BioMax XAR; Kodak, USA).

Immunoprecipitation and western blot analysis

5×10^6 KG1a cells were lysed in lysis buffer B (50 mM HEPES pH 7.5, 150 mM NaCl, 1.5 mM $MgCl_2$, 1 mM EDTA, 10% glycerol, 1% Triton X-100, 1 mM PMSF, 1 μg/ml leupeptin and aprotinin). Immunoprecipitations were carried out with 1 μg of AZN-L51 antibody coupled to Protein G Sepharose 4 Fast Flow beads. Bound proteins were eluted by boiling in Laemmli sample buffer, subjected to 12% SDS-PAGE under reducing conditions and transferred onto a nitrocellulose membrane. To detect ALCAM and actin, membranes were incubated for 1 hour with AZN-L50 or mouse monoclonal anti-β-actin (Sigma), followed by 1-hour incubation with a peroxidase-conjugated rabbit anti-mouse IgG (DAKO, Denmark) and proteins were visualized using an enhanced chemiluminescence system (Amersham Biosciences).

AFM force measurements

Force measurements were made on living cells in force-distance mode (Fig. 1) using a MultiMode AFM (Nanoscope IIIa) equipped with a 'J'-type piezoelectric translator (Veeco Instruments, Santa Barbara, CA). Triangular gold-coated silicon-nitride cantilevers were used with a nominal spring constant of 10 pN/nm as given by the manufacturer (MLCT-AUHW, Veeco Instruments). Cantilever deflection was determined from the difference in signal generated by a two-segment photodiode monitoring the reflection of a laser beam focused onto the endpoint of the cantilever (Fig. 1B). Each cantilever was calibrated before use by a nondestructive thermal oscillation method (Hutter and Bechhoefer, 1993); by using this method the uncertainty in the determination of the spring constant amounted to 3-4% per cantilever. The experimentally determined spring constants of the used cantilevers were 15±2 pN/nm, and these values were used to obtain interaction forces using Hooke's law, $F=k\times\Delta x$. Here, F is the force (expressed in piconewtons, pN), k is the experimentally obtained spring constant (pN/nm), and Δx is the measured cantilever deflection (nm).

Protein immobilization

ALCAM-Fc and CD6-Fc were immobilized on 13 mm plastic coverslips (Nalge Nunc, Rochester, NY). First, in an overnight (4°C) incubation, 10 μg/ml goat anti-human Fc-$(Fab')_2$ fragments were absorbed to the coverslip surface in TSM (20 mM Tris, 150 mM NaCl, 1 mM $CaCl_2$, 2 mM $MgCl_2$, pH 8.0). Then the substrates were rinsed and subsequently incubated for 30 minutes in TSM/1% (w/v) BSA at 37°C to block the remaining exposed non-coated surface. After an additional washing step, the plates were incubated with 5 μg/ml ALCAM-Fc or 5 μg/ml CD6-Fc in TSM for 1 hour at 37°C. Finally, the coated substrates were washed and transferred into the AFM measuring chamber (MTFML, Veeco Instruments).

Functionalization of AFM cantilevers with cells

Cells were attached to the AFM cantilever by concanavalin A (ConA)-mediated linkages essentially as described previously (Wojcikiewicz et al., 2003). ConA-coated cantilevers were prepared as follows. Cantilevers were first cleaned by immersion in acetone for 5 minutes, then rinsed with ethanol and subsequently dried in a microwave oven. Following an overnight incubation at 37°C in biotinylated BSA (biotin-BSA, 0.5 mg/ml in 100 mM $NaHCO_3$, pH 8.6) the cantilevers were rinsed using PBS and exposed to 0.5 mg/ml (PBS, 30 minutes, 37°C) streptavidin (Pierce, Rockford, IL). Finally, the cantilevers were incubated in biotinylated ConA (biotin-ConA, 0.2 mg/ml in PBS) for 30 minutes at 37°C and washed with PBS.

Cells kept in medium A (RPMI 1640, 10% FCS, 25 mM HEPES; pH 7.0) were seeded onto a clean uncoated glass coverslip and were picked up under the guidance of an optical microscope mounted on top of the AFM, using the AFM as a micromanipulator. For this, the ConA-functionalized cantilever was positioned over a target cell on the substrate and was approached to establish contact lasting at least one minute. During this time the applied indentation force was kept constant at about 2.5 nN. Upon retraction, the successful pick-up was readily scored by visual inspection, and, in these events, the cell was positioned right behind the AFM tip (Fig. 1C).

Rupture-force measurements and force spectroscopy

The cell-bearing cantilever was brought into contact with the ligand-coated substrate (Fig. 1Ba-c) for a preset period of time (interaction time; 25°C, medium A). During this time, a force was exerted on the cell of no more than ~1 nN. Interaction times were such that a minimal, yet significant, ALCAM-specific adhesion was established (typically between 0.5-3.0 seconds, see Results). Upon retraction, the forces acting on the cantilever were recorded as a function of displacement of the ALCAM–CD6-coated substrate (Fig. 1Bd-f, Fig. 1D). ALCAM-ALCAM and ALCAM-CD6 rupture forces were determined directly from the height of the sudden variations in binding force that are associated with bond rupture. The final ruptures in the force-distance curves were used for further analysis (Fig. 1D; see below). The area enclosed by the zero-force axis and the force-distance curve (Fig. 1D) was taken as a measure for the work ($W=F\times d$) performed during the detachment phase (Zhang et al., 2002; Puech et al., 2005). CytD treatments were performed in situ (2.5 μg/ml in medium A, 25 minutes). Specificity was verified by an in situ incubation with the function-blocking ALCAM-specific monoclonal antibody AZN-L50 (10 μg/ml, 25 minutes). Force curves were analyzed using Origin Pro 6.1 (OriginLab Corporation, Northampton, MA). The same package was used for performing Student's t-test.

Force spectroscopy was applied to study how the rupture forces depend on the loading rate (i.e. the rate at which force builds up on the respective bonds). Loading rates (pN/second) were computed as the product of the slope of the force-distance curve (pN/nm) just before a rupture event – the effective force constant that takes the viscoelastic properties of the system into account (Evans and Ritchie, 1999; Yuan et al., 2000) – and the pulling velocity (nm/second). Pulling velocities were varied from 250-12,500 nm/second. The final ruptures in the force-distance curves were used for further analysis and for each of these events both the loading rate and the rupture force was determined (Fig. 1D). For each cell, complete force spectra were recorded under identical conditions on both substrates by switching the ligand-coated plate for one containing the other. Pulling rates were varied randomly and reproducibility over time was verified by repeating measurements using prior pulling-rate settings. After each series, ALCAM specificity of the adhesion was checked using the blocking mAb AZN-L50.

At retraction speeds >1 μm/second, the hydrodynamic drag on the cantilever resulted in damping and, as a result, smaller forces were recorded than were actually applied to rupture the bonds (Evans et al., 2001; Tees et al., 2001; Zhang et al., 2002). To compensate for this effect, the data were corrected using a damping coefficient of 2 pN second/μm.

J.t.R. is supported by NanoNed, the Dutch nanotechnology programme of the Ministry of Economic Affairs. The Netherlands Organization of Scientific Research supports C.G.F. through TOP Grant 9120.6030 and A.C. through Grant Veni 916.66.028 and SLW 33.302P. F.d.L. received support through grant KUN OZ-2002-5 from the Radboud University Nijmegen Medical Centre. The authors thank Ben Ohler and Patrick Markus (Veeco Instruments) for their valuable technical support, and Peter Schön for critical reading of the manuscript. The Microscopic Imaging Centre (MIC) of the NCMLS is kindly acknowledged for providing facilities.

References

Alon, R., Chen, S., Fuhlbrigge, R., Puri, K. D. and Springer, T. A. (1998). The kinetics and shear threshold of transient and rolling interactions of L-selectin with its ligand on leukocytes. *Proc. Natl. Acad. Sci. USA* **95**, 11631-11636.

Bell, G. I. (1978). Models for the specific adhesion of cells to cells. *Science* **200**, 618-627.

Benoit, M., Gabriel, D., Gerisch, G. and Gaub, H. E. (2000). Discrete interactions in cell adhesion measured by single-molecule force spectroscopy. *Nat. Cell Biol.* **2**, 313-317.

Bhasin, N., Carl, P., Harper, S., Feng, G., Lu, H., Speicher, D. W. and Discher, D. E. (2004). Chemistry on a single protein, vascular cell adhesion molecule-1, during forced unfolding. *J. Biol. Chem.* **279**, 45865-45874.

Binnig, G., Quate, C. F. and Gerber, C. (1986). Atomic force microscope. *Phys. Rev. Lett.* **56**, 930-933.

Bowen, M. A., Patel, D. D., Li, X., Modrell, B., Malacko, A. R., Wang, W. C., Marquardt, H., Neubauer, M., Pesando, J. M. and Francke, U. (1995). Cloning, mapping, and characterization of activated leukocyte-cell adhesion molecule (ALCAM), a CD6 ligand. *J. Exp. Med.* **181**, 2213-2220.

Bowen, M. A., Aruffo, A. A. and Bajorath, J. (2000). Cell surface receptors and their ligands: in vitro analysis of CD6-CD166 interactions. *Proteins* **40**, 420-428.

Cambi, A., de Lange, F., van Maarseveen, N. M., Nijhuis, M., Joosten, B., van Dijk, E. M., de Bakker, B. I., Fransen, J. A., Bovee-Geurts, P. H., van Leeuwen, F. N.

et al. (2004). Microdomains of the C-type lectin DC-SIGN are portals for virus entry into dendritic cells. *J. Cell Biol.* **164**, 145-155.

Cambi, A., Joosten, B., Koopman, M., de Lange, F., Beeren, I., Torensma, R., Fransen, J. A., Garcia-Parajo, M., van Leeuwen, F. N. and Figdor, C. G. (2006). Organization of the integrin LFA-1 in nanoclusters regulates its activity. *Mol. Biol. Cell* **17**, 4270-4281.

Carl, P., Kwok, C. H., Manderson, G., Speicher, D. W. and Discher, D. E. (2001). Forced unfolding modulated by disulfide bonds in the Ig domains of a cell adhesion molecule. *Proc. Natl. Acad. Sci. USA* **98**, 1565-1570.

Carman, C. V. and Springer, T. A. (2003). Integrin avidity regulation: are changes in affinity and conformation underemphasized? *Curr. Opin. Cell Biol.* **15**, 547-556.

Chen, A. and Moy, V. T. (2000). Cross-linking of cell surface receptors enhances cooperativity of molecular adhesion. *Biophys. J.* **78**, 2814-2820.

Cowin, P., Rowlands, T. M. and Hatsell, S. J. (2005). Cadherins and catenins in breast cancer. *Curr. Opin. Cell Biol.* **17**, 499-508.

Degen, W. G., van Kempen, L. C., Gijzen, E. G., van Groningen, J. J., van Kooyk, Y., Bloemers, H. P. and Swart, G. W. (1998). MEMD, a new cell adhesion molecule in metastasizing human melanoma cell lines, is identical to ALCAM (activated leukocyte cell adhesion molecule). *Am. J. Pathol.* **152**, 805-813.

Evans, E. and Ritchie, K. (1997). Dynamic strength of molecular adhesion bonds. *Biophys. J.* **72**, 1541-1555.

Evans, E. and Ritchie, K. (1999). Strength of a weak bond connecting flexible polymer chains. *Biophys. J.* **76**, 2439-2447.

Evans, E., Leung, A., Hammer, D. and Simon, S. (2001). Chemically distinct transition states govern rapid dissociation of single L-selectin bonds under force. *Proc. Natl. Acad. Sci. USA* **98**, 3784-3789.

Evans, E., Heinrich, V., Leung, A. and Kinoshita, K. (2005). Nano- to microscale dynamics of P-selectin detachment from leukocyte interfaces. I. Membrane separation from the cytoskeleton. *Biophys. J.* **88**, 2288-2298.

Gangemi, R. M., Swack, J. A., Gaviria, D. M. and Romain, P. L. (1989). Anti-T12, an anti-CD6 monoclonal antibody, can activate human T lymphocytes. *J. Immunol.* **143**, 2439-2447.

Gimferrer, I., Calvo, M., Mittelbrunn, M., Farnos, M., Sarrias, M. R., Enrich, C., Vives, J., Sanchez-Madrid, F. and Lozano, F. (2004). Relevance of CD6-mediated interactions in T cell activation and proliferation. *J. Immunol.* **173**, 2262-2270.

Gimferrer, I., Ibanez, A., Farnos, M., Sarrias, M. R., Fenutria, R., Rosello, S., Zimmermann, P., David, G., Vives, J., Serra-Pages, C. et al. (2005). The lymphocyte receptor CD6 interacts with syntenin-1, a scaffolding protein containing PDZ domains. *J. Immunol.* **175**, 1406-1414.

Grakoui, A., Bromley, S. K., Sumen, C., Davis, M. M., Shaw, A. S., Allen, P. M. and Dustin, M. L. (1999). The immunological synapse: a molecular machine controlling T cell activation. *Science* **285**, 221-227.

Hanahan, D. and Weinberg, R. A. (2000). The hallmarks of cancer. *Cell* **100**, 57-70.

Hanley, W., McCarty, O., Jadhav, S., Tseng, Y., Wirtz, D. and Konstantopoulos, K. (2003). Single molecule characterization of P-selectin/ligand binding. *J. Biol. Chem.* **278**, 10556-10561.

Hanley, W. D., Wirtz, D. and Konstantopoulos, K. (2004). Distinct kinetic and mechanical properties govern selectin-leukocyte interactions. *J. Cell Sci.* **117**, 2503-2511.

Hassan, N. J., Barclay, A. N. and Brown, M. H. (2004). Frontline: optimal T cell activation requires the engagement of CD6 and CD166. *Eur. J. Immunol.* **34**, 930-940.

Hazan, R. B., Qiao, R., Keren, R., Badano, I. and Suyama, K. (2004). Cadherin switch in tumor progression. *Ann. N. Y. Acad. Sci.* **1014**, 155-163.

Hinterdorfer, P. (2002). Molecular recognition studies using the atomic force microscope. *Methods Cell Biol.* **68**, 115-139.

Hinterdorfer, P. and Dufrêne, Y. F. (2006). Detection and localization of single molecular recognition events using atomic force microscopy. *Nat. Methods* **3**, 347-355.

Hummer, G. and Szabo, A. (2001). Free energy reconstruction from nonequilibrium single-molecule pulling experiments. *Proc. Natl. Acad. Sci. USA* **98**, 3658-3661.

Hutter, J. L. and Bechhoefer, J. (1993). Calibration of atomic-force microscope tips. *Rev. Sci. Instrum.* **64**, 1868-1873.

Kashiwagi, H., Kijima, H., Dowaki, S., Ohtani, Y., Tobita, K., Yamazaki, H., Nakamura, M., Ueyama, Y., Tanaka, M., Inokuchi, S. et al. (2004). Clinicopathological significance of sialyl Lex expression in human gallbladder carcinoma. *Oncol. Rep.* **11**, 1139-1143.

Kim, K. D., Choi, S. C., Noh, Y. W., Kim, J. W., Paik, S. G., Yang, Y., Kim, K., 2nd and Lim, J. S. (2006). Impaired responses of leukemic dendritic cells derived from a human myeloid cell line to LPS stimulation. *Exp. Mol. Med.* **38**, 72-84.

Kim, M., Carman, C. V., Yang, W., Salas, A. and Springer, T. A. (2004). The primacy of affinity over clustering in regulation of adhesiveness of the integrin $\alpha_L\beta_2$. *J. Cell Biol.* **167**, 1241-1253.

King, J. A., Ofori-Acquah, S. F., Stevens, T., Al-Mehdi, A. B., Fodstad, O. and Jiang, W. G. (2004). Activated leukocyte cell adhesion molecule in breast cancer: prognostic indicator. *Breast Cancer Res.* **6**, R478-R487.

Knudsen, K. A. and Wheelock, M. J. (2005). Cadherins and the mammary gland. *J. Cell. Biochem.* **95**, 488-496.

Kristiansen, G., Pilarsky, C., Wissmann, C., Stephan, C., Weissbach, L., Loy, V., Loening, S., Dietel, M. and Rosenthal, A. (2003). ALCAM/CD166 is up-regulated in low-grade prostate cancer and progressively lost in high-grade lesions. *Prostate* **54**, 34-43.

Li, F., Redick, S. D., Erickson, H. P. and Moy, V. T. (2003). Force measurements of the $\alpha_5\beta_1$ integrin-fibronectin interaction. *Biophys. J.* **84**, 1252-1262.

Li, G., Satyamoorthy, K., Meier, F., Berking, C., Bogenrieder, T. and Herlyn, M. (2003). Function and regulation of melanoma-stromal fibroblast interactions: when seeds meet soil. *Oncogene* **22**, 3162-3171.

Lunter, P. C., van Kilsdonk, J. W., van Beek, H., Cornelissen, I. M., Bergers, M., Willems, P. H., van Muijen, G. N. and Swart, G. W. (2005). Activated leukocyte cell adhesion molecule (ALCAM/CD166/MEMD), a novel actor in invasive growth, controls matrix metalloproteinase activity. *Cancer Res.* **65**, 8801-8808.

Masedunskas, A., King, J. A., Tan, F., Cochran, R., Stevens, T., Sviridov, D. and Ofori-Acquah, S. F. (2006). Activated leukocyte cell adhesion molecule is a component of the endothelial junction involved in transendothelial monocyte migration. *FEBS Lett.* **580**, 2637-2645.

Mempel, T. R., Henrickson, S. E. and Von Andrian, U. H. (2004). T-cell priming by dendritic cells in lymph nodes occurs in three distinct phases. *Nature* **427**, 154-159.

Nelissen, J. M., Peters, I. M., de Grooth, B. G., van Kooyk, Y. and Figdor, C. G. (2000). Dynamic regulation of activated leukocyte cell adhesion molecule-mediated homotypic cell adhesion through the actin cytoskeleton. *Mol. Biol. Cell* **11**, 2057-2068.

Osorio, L. M., Rottenberg, M., Jondal, M. and Chow, S. C. (1998). Simultaneous cross-linking of CD6 and CD28 induces cell proliferation in resting T cells. *Immunology* **93**, 358-365.

Panorchan, P., George, J. P. and Wirtz, D. (2006a). Probing intercellular interactions between vascular endothelial cadherin pairs at single-molecule resolution and in living cells. *J. Mol. Biol.* **358**, 665-674.

Panorchan, P., Thompson, M. S., Davis, K. J., Tseng, Y., Konstantopoulos, K. and Wirtz, D. (2006b). Single-molecule analysis of cadherin-mediated cell-cell adhesion. *J. Cell Sci.* **119**, 66-74.

Patel, D. D., Wee, S. F., Whichard, L. P., Bowen, M. A., Pesando, J. M., Aruffo, A. and Haynes, B. F. (1995). Identification and characterization of a 100-kD ligand for CD6 on human thymic epithelial cells. *J. Exp. Med.* **181**, 1563-1568.

Puech, P. H., Taubenberger, A., Ulrich, F., Krieg, M., Muller, D. J. and Heisenberg, C. P. (2005). Measuring cell adhesion forces of primary gastrulating cells from zebrafish using atomic force microscopy. *J. Cell Sci.* **118**, 4199-4206.

Quentmeier, H., Duschl, A., Hu, Z. B., Schnarr, B., Zaborski, M. and Drexler, H. G. (1996). MUTZ-3, a monocytic model cell line for interleukin-4 and lipopolysaccharide studies. *Immunology* **89**, 606-612.

Rasmussen, R. A., Counts, S. L., Daley, J. F. and Schlossman, S. F. (1994). Isolation and characterization of $CD6^-$ T cells from peripheral blood. *J. Immunol.* **152**, 527-536.

Rief, M. and Grubmüller, H. (2002). Force spectroscopy of single biomolecules. *Chemphyschem* **3**, 255-261.

Swart, G. W. (2002). Activated leukocyte cell adhesion molecule (CD166/ALCAM): developmental and mechanistic aspects of cell clustering and cell migration. *Eur. J. Cell Biol.* **81**, 313-321.

Swart, G. W., Lunter, P. C., Kilsdonk, J. W. and Kempen, L. C. (2005). Activated leukocyte cell adhesion molecule (ALCAM/CD166): signaling at the divide of melanoma cell clustering and cell migration? *Cancer Metastasis Rev.* **24**, 223-236.

Tanaka, H., Matsui, T., Agata, A., Tomura, M., Kubota, I., McFarland, K. C., Kohr, B., Lee, A., Phillips, H. S. and Shelton, D. L. (1991). Molecular cloning and expression of a novel adhesion molecule, SC1. *Neuron* **7**, 535-545.

Tees, D. F., Waugh, R. E. and Hammer, D. A. (2001). A microcantilever device to assess the effect of force on the lifetime of selectin-carbohydrate bonds. *Biophys. J.* **80**, 668-682.

Tomita, K., van Bokhoven, A., Jansen, C. F. J., Kiemeney, L. A., Karthaus, H. F. M., Vriesema, J., Bussemakers, M. J. G., Witjes, J. A. and Schalken, J. A. (2003). Activated Leukocyte Cell Adhesion Molecule (ALCAM) expression is associated with a poor prognosis for bladder cancer patients. *UroOncology* **3**, 121-129.

Uhlenbrock, K., Eberth, A., Herbrand, U., Daryab, N., Stege, P., Meier, F., Friedl, P., Collard, J. G. and Ahmadian, M. R. (2004). The RacGEF Tiam1 inhibits migration and invasion of metastatic melanoma via a novel adhesive mechanism. *J. Cell Sci.* **117**, 4863-4871.

van Kempen, L. C., van den Oord, J. J., van Muijen, G. N., Weidle, U. H., Bloemers, H. P. and Swart, G. W. (2000). Activated leukocyte cell adhesion molecule/CD166, a marker of tumor progression in primary malignant melanoma of the skin. *Am. J. Pathol.* **156**, 769-774.

van Kempen, L. C., Nelissen, J. M., Degen, W. G., Torensma, R., Weidle, U. H., Bloemers, H. P., Figdor, C. G. and Swart, G. W. (2001). Molecular basis for the homophilic activated leukocyte cell adhesion molecule (ALCAM)-ALCAM interaction. *J. Biol. Chem.* **276**, 25783-25790.

van Kooyk, Y. and Figdor, C. G. (2000). Avidity regulation of integrins: the driving force in leukocyte adhesion. *Curr. Opin. Cell Biol.* **12**, 542-547.

Wee, S., Schieven, G. L., Kirihara, J. M., Tsu, T. T., Ledbetter, J. A. and Aruffo, A. (1993). Tyrosine phosphorylation of CD6 by stimulation of CD3: augmentation by the CD4 and CD2 coreceptors. *J. Exp. Med.* **177**, 219-223.

Weichert, W., Knosel, T., Bellach, J., Dietel, M. and Kristiansen, G. (2004). ALCAM/CD166 is overexpressed in colorectal carcinoma and correlates with shortened patient survival. *J. Clin. Pathol.* **57**, 1160-1164.

Willemsen, O. H., Snel, M. M., Cambi, A., Greve, J., De Grooth, B. G. and Figdor, C. G. (2000). Biomolecular interactions measured by atomic force microscopy. *Biophys. J.* **79**, 3267-3281.

Wojcikiewicz, E. P., Zhang, X., Chen, A. and Moy, V. T. (2003). Contributions of molecular binding events and cellular compliance to the modulation of leukocyte adhesion. *J. Cell Sci.* **116**, 2531-2539.

Wong, J., Chilkoti, A. and Moy, V. T. (1999). Direct force measurements of the streptavidin-biotin interaction. *Biomol. Eng.* **16**, 45-55.

Yuan, C., Chen, A., Kolb, P. and Moy, V. T. (2000). Energy landscape of streptavidin-biotin complexes measured by atomic force microscopy. *Biochemistry* **39**, 10219-10223.

Zhang, X., Wojcikiewicz, E. P. and Moy, V. T. (2002). Force spectroscopy of the

leukocyte function-associated antigen-1/intercellular adhesion molecule-1 interaction. *Biophys. J.* **83**, 2270-2279.

Zhang, X., Bogorin, D. F. and Moy, V. T. (2004a). Molecular basis of the dynamic strength of the sialyl Lewis X-selectin interaction. *Chemphyschem* **5**, 175-182.

Zhang, X., Craig, S. E., Kirby, H., Humphries, M. J. and Moy, V. T. (2004b). Molecular basis for the dynamic strength of the integrin $\alpha_4\beta_1$/VCAM-1 interaction. *Biophys. J.* **87**, 3470-3478.

Zimmerman, A. W., Nelissen, J. M., Van Emst-De Vries, S. E., Willems, P. H., De Lange, F., Collard, J. G., Van Leeuwen, F. N. and Figdor, C. G. (2004). Cytoskeletal restraints regulate homotypic ALCAM-mediated adhesion through PKCα independently of Rho-like GTPases. *J. Cell Sci.* **117**, 2841-2852.

Zimmerman, A. W., Joosten, B., Torensma, R., Parnes, J. R., van Leeuwen, F. N. and Figdor, C. G. (2006). Long-term engagement of CD6 and ALCAM is essential for T-cell proliferation induced by dendritic cells. *Blood* **107**, 3212-3220.